ELSEVIER

Journal of Alloys and Compounds 461 (2008) 321–325

Journal of ALLOYS AND COMPOUNDS

www.elsevier.com/locate/jallcom

A new composite anode, Fe–Cu–Si/C for lithium ion battery

Chil-Hoon Doh [a,*], Hye-Min Shin [a,b], Dong-Hun Kim [a,c], Young-Dong Jeong [a], Seong-In Moon [a], Bong-Soo Jin [a], Hyun-Soo Kim [a], Ki-Won Kim [c], Dae-Hee Oh [b], Angathevar Veluchamy [a,d]

[a] *Korea Electrotechnology Research Institute, Changwon 641 600, Republic of Korea*
[b] *Pukyong National University, Pusan 608 739, Republic of Korea*
[c] *Gyeonsang National University, Jinju 660 701, Republic of Korea*
[d] *Central Electrochemical Research Institute, Karaikudi 630 006, India*

Received 20 April 2007; received in revised form 12 June 2007; accepted 23 June 2007
Available online 28 July 2007

Abstract

A new anode composite material comprising Fe, Cu and Si in conjunction with graphite has been obtained through high energy ball milling (HEBM) technique. The X-ray diffraction (XRD) analysis predicts that the milled composite particles remain in the elemental state and the scanning electron microscope (SEM) pictures show that the electrode annealed at 200 °C consists of well-defined aggregate particulates with interspaces. The composite electrode exhibits high initial discharge and charge capacity of 809 and 464 mAh g^{-1}, respectively with a sustainable reversible capacity >385 mAh g^{-1} at 30th cycle and maintains high coulombic efficiency >95% after 4th cycle. As the annealing temperature is changed from 110 to >150 °C, the irreversible capacity increased from 158 to 340 mAh g^{-1}.

Keywords: High energy mechanical milling; Fe–Cu–Si/graphite composite; Anode; Li-ion battery; Irreversible capacity loss

1. Introduction

The exponential growth of electronic industry demands compact lithium ion power packs which necessitates development of high energy electrode materials. Recently it has been found that tin (Sn) and silicon (Si) were able to form intermetallic alloys such as $Li_{22}Si_5$ and $Li_{22}Sn_5$ with lithium giving theoretical capacities 4190 and 990 mAh g^{-1}, and volume variations 328 and 258% based on crystal parameters, respectively. Despite their high energy density, the direct use of the materials as anode is hampered due to wide volume variations during charge/discharge process. Such volume variation causes stress within the electrode leading to internal cracks and morphological changes resulting in loss of electrical contact and cell failure [1].

In order to harness the high theoretical energy density of silicon, a host of metals and carbons were considered along with silicon to arrive at an optimum composition which could lead to low volume change during alloying and de-alloying, in addition to providing high energy density than that of presently employed graphite anode [2].

In this attempt intermetallic silicide alloys with less active or inactive metal elements with binary alloys such as Ca–Si [3], Ni–Si [4–9], Fe–Si [10–12], Mn–Si [13–15], Co–Si [16], Mg–Si [17,18], Cu–Si [19–22], Ag–Si [23], Ti–Si [24], Ti–C [25]. Cr–Si [26] and also alloys consisting of multicomponents Si–M (M = Cr + Ni, Fe, Mn) [27], Si–Ba–Fe [28], Si–Nd–Fe–B [29], Si–Fe–Mn [30] and Si–AB_5 (MmNi, Co, Al, Mn) [31] were explored mostly with graphite. Among these compositions, there were reports on the exploitation of Fe or Cu for the development of composite anodes along with Si. For example, Lee and Lee [10] reported the synthesis of Fe–Si/graphite anode through high energy ball milling (HEBM) where the formed product $FeSi_2$ was considered as playing the role of buffer to sustain a reversible capacity, 600 mAh g^{-1} even at 20th cycle. The irreversible capacity observed mainly between 0.9 and 0.7 V was supposed to be caused by electrolyte decomposition and passive film formation on the carbon particles. Around 200 compositions of combinatorial materials comprising Si–M (M = Cr + Ni, Fe, Mn) has been reported [27] where the anode capacity strongly depended upon Si content varying from over 3000 mAh g^{-1} for nearly pure silicon to

* Corresponding author. Tel.: +82 55 280 1662; fax: +82 55 280 1590.
E-mail address: chdoh@keri.re.kr (C.-H. Doh).

0925-8388/$ – see front matter © 2007 Elsevier B.V. All rights reserved.
doi:10.1016/j.jallcom.2007.06.125

effectively zero around 50–60 at% of silicon. Multiple component alloy composite [28] with carbon/Ba–Fe–Si alloy has been observed to provide 500 mAh g^{-1} at 15th cycle. A magnetic alloy comprising of Si–Nd–Fe–B [29] as an anode was found to deliver intercalation capacity of 831 mAh g^{-1} while providing reversible capacity of 352 mAh g^{-1} at 30th cycle. On the possibility of using $LiFePO_4$ and $Fe_{0.92}Mn_{0.08}Si_2$ as anode materials, reversible capacity of ~300 and ~400 mAh g^{-1} at 20th and 25th cycles, respectively, were reported [30,32]. Si–AB_5 composite alloy [31], where Fe is one of the components, exhibited initial and maximum reversible capacity of 370 and 385 mAh g^{-1} with high capacity retention even after 50 cycles. Similarly the role of copper has been explored in anode compositions. NuLi et al. [20] reported for Cu_5Si–Si/C anode, a capacity around 612 mAh g^{-1} and explain the capacity fade at the initial cycles as due to SEI film formation. A similar composition containing Si, Si/Cu core in carbon shell composite anode synthesized through inversion emulsion polymerization of resorcinol–formaldehyde Wang et al. [22] reported an initial reversible and 20th cycle capacity as 910 and ~800 mAh g^{-1}, respectively.

The composite alloy anodes explored so far contain either Cu or Fe along with silicon, graphite and other elements, and no reports are available where both elements are present in one composition. Hence this paper is the result of an attempt to prepare a composite alloy comprising both Fe, Cu along with Si in the atomic ratio Fe:Cu:Si = 1:1:2.5. As this composition has been explored with graphite (C), the final composition "Fe:Cu:Si = 1:1:2.5/graphite" may be denoted as Fe–Cu–Si/C. The synthesis procedure uses high energy ball mill technique (HEBM) to prepare Fe–Cu–Si/C composite. Techniques such as X-ray diffraction (XRD) and scanning electron microscope (SEM) were employed to analyze the structure and morphology of the materials.

2. Experimental details

2.1. Material preparation

Appropriate quantities of Cu (<10 μm, 99% pure, Sigma–Aldrich), Fe (<53 μm, 99.9% pure, High Purity Chemical Research Company, Japan) and Si (1–5 μm, SI-100, >99 purity, AEE, NJ) with atomic ratio, Fe:Cu:Si = 1:1:2.5 (denoted as Fe–Cu–Si) were weighed and loaded into a stainless steel (SS) grinding vial along with SS balls. The weight ratio of SS ball to material was maintained at 10:1 and all the millings were carried out at 350 rpm. The vial was filled with argon gas and the vial tightly closed with a gasket provision to prevent the oxidation of the loaded material by any ingress of atmospheric air into the vial. Two materials, one ball milled for 3 h and another one milled for 10 h were carried out in order to compare the effect of ball milling over the composite mix. The material ball milled for 3 h was then mixed with graphite in equal proportions (50:50) in weight ratio and again ball milled for 24 h. Thus prepared active material was then blended with 10 wt% polyvinylidene difluoride (PVDF) dissolved in 1-methyl-2-pyrrolidinone using an agitator for 10 min. The slurry mass was coated onto a copper foil current collector and dried in a hot air oven at 110 °C for 2 h. In order to reinforce the active material coating over copper foil, the coated films were pressed using a SS roller and the thickness was reduced to about ~75%. The pressed films were annealed at 110, 150, 200, and 250 °C for 12 h in vacuum to explore the effect of temperature on the capacity and cycling behavior of the anode material. Herein after 3, 10, and 24 h ball milled materials will be referred to as 3HBM, 10HBM, and 24HBM, respectively.

2.2. Cell construction

The active material was coated with copper foil cut in the form of a circular disc of diameter 1.4 cm and coupled with lithium foil counter electrode separated by © membrane 2700 polypropylene separator. The electrolyte (received from Techno Semichem. Ltd., Korea) is made up of 1 M $LiPF_6$ dissolved in a co-solvent consisting of ethylene carbonate (EC) and ethyl methyl carbonate (EMC) in 1:1 (v/v) ratio with 2 wt% vinylene carbonate (VC). The coin cells were assembled in a dry room maintained at ~21 °C with dew point temperature between 65 and 70 °C.

2.3. XRD and SEM investigations

In order to obtain the phase characterization, ball milled composites were examined using Philips 1830 X-ray diffractometer with nickel filtered Cu Kα radiation at a scan rate of 0.04°/s over 2θ range 10–80°. The surface morphology of the active material coated copper foil was scanned using Hitachi S-4800 scanning electron microscope.

2.4. Cycle life testing

Discharge–charge studies and cycle life measurements of the coin cells were carried out using charge–discharge analyzer, Toyo System, Ltd., Japan. The anode was cycled between 0 and 2 V versus Li^+/Li at a constant current of 0.253 mA cm^{-2}.

3. Results and discussion

3.1. Phase and morphology analyses

3.1.1. X-ray diffraction of the ball milled sample

In Fig. 1, the XRD pattern for Si, Cu, Fe, graphite powder (C), 3HBM-Fe–Cu–Si, 10HBM-Fe–Cu–Si, and 24HBM-{3HBM-Fe–Cu–Si:graphite = 50:50 (w/w)} are presented. The superimposition of Braggs peaks appearing in the XRD pattern of individual materials such as Si, Cu, Fe and Si, Cu, Fe and graphite shows that the superimposed XRD spectrum coincide exactly with spectra obtained for 3HBM-Fe–Cu–Si, 10HBM-Fe–Cu–Si, and 24HBM-{3HBM-Fe–Cu–Si:graphite = 50:50 (w/w)}, respectively. All these suggest that the duration of ball milling could not impact effectively on the elemental particles to produce any alloy formation, rather reduced them into smaller particulates as evident from the minimum change in the intensity of Braggs peak in the XRD patterns.

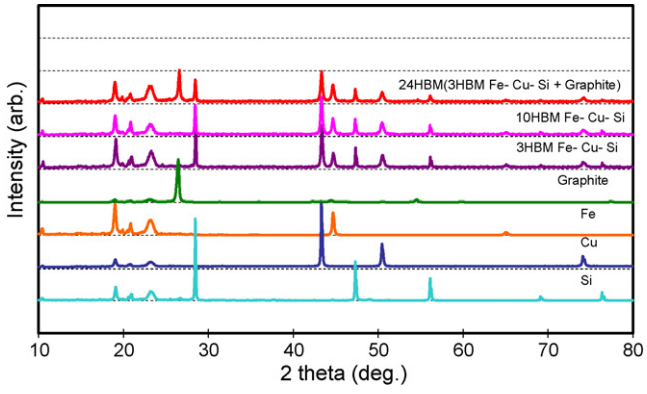

Fig. 1. XRD pattern of Fe, Cu, Si, C, 3HBM-Fe–Cu–Si, 10HBM-Fe–Cu–Si, and 24HBM-{3HBM-Fe–Cu–Si:C = 50:50 (w/w)}.

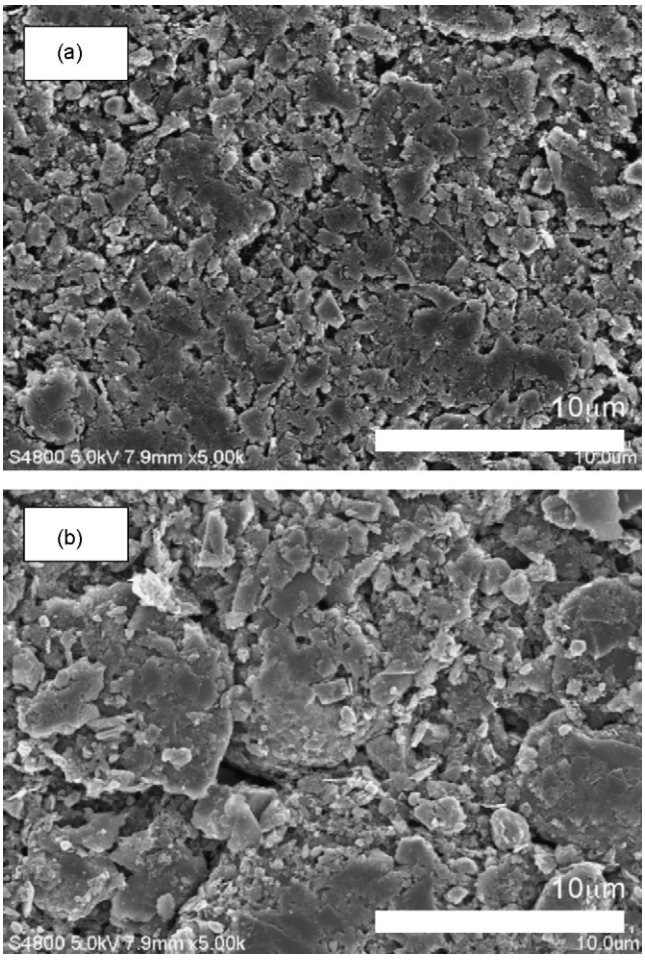

Fig. 2. SEM pictures of Fe–Cu–Si/C composite electrode with PVDF binder annealed at (a) 110 °C and (b) 200 °C.

3.1.2. SEM analysis

The SEM pictures of Fe–Cu–Si/C with PVDF binder annealed at 110 °C was compared with the best performing electrode annealed at 200 °C and presented in Fig. 2 as 'a' and 'b', respectively. The pictures show the cathode particles in 'b' remain as well defined agglomerate particles with distinct interspaces compared to that of the particles in 'a' with particle sizes varying from <1 to ~10 μm. The high temperature treatment would have impacted agglomeration and segregation of the particles aided by PVDF binder resulting in the formation of interspaces. Formation of such interfaces may be expected to aid better buffer action to absorb the volume change of the electrode during charge/discharge cycles.

3.2. Electrochemical characterization

3.2.1. Discharge/charge behavior

The typical discharge–charge profiles for Fe–Cu–Si/C composite electrode annealed at 200 °C is presented as in Fig. 3. The figure shows initial lithiation (discharge) and delithiation (charge) capacities are 809 and 464 mAh g^{-1}, respectively. The capacity difference between the two processes is 345 mAh which is nearly 42% of the initial lithiation capacity. This implies that

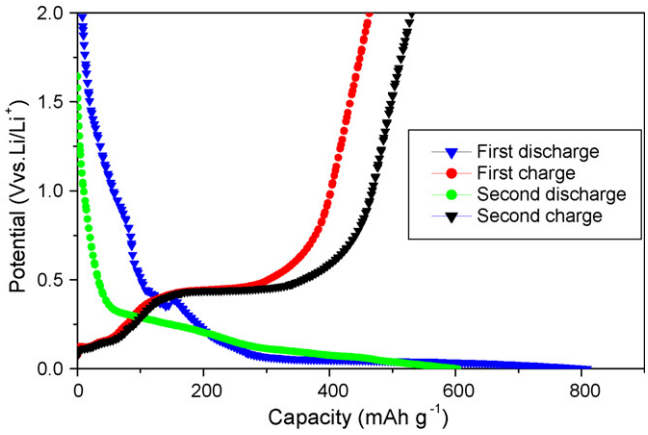

Fig. 3. Discharge–charge profiles for Fe–Cu–Si/C composite electrode annealed at 200 °C.

during the first cycle about 42% of lithium is retained within the electrode as irreversible capacity. Not only the graphite carbons but also the metal particles and silicon present in the composite will have chemically bonded or adsorbed oxides over their surfaces. Initially during first discharge the inserted lithium reacts irreversibly with these oxides and water molecules leading to the formation of Li_2O, and then forms Li–Si alloy and LiC_6. Formation of Li_2O accounts for the large irreversible capacity during the first cycle. The formed Li_2O along with Fe, Cu and graphite acts as a buffer to absorb the volume expansion/contraction during discharge/charge process. Also other products formed along with Li_2O due to the oxidation of electrolyte and binder act as a passivation film around the electro-active particles such as silicon and graphite.

For the present system we propose the following reaction mechanism that account for the lithiation (discharge)/delithiation (charge) process, irreversible capacity and capacity degradation with cycle life.

(1) The charge/discharge reversible reaction

$$(x+y)\mathrm{Li}^+ + (\mathrm{Si},\ \mathrm{Fe},\ \mathrm{Cu},\ \mathrm{C}) + (x+y)\mathrm{e}^- \leftrightarrow \mathrm{Li}_x\mathrm{Si} + \mathrm{Li}_y\mathrm{C}_6 + (\mathrm{Fe},\ \mathrm{Cu}) \quad (1)$$

(2) The irreversible reaction during initial discharge

$$2\mathrm{Li}^+ + {-}\mathrm{O}{-} + 2\mathrm{e}^- \rightarrow \mathrm{Li}_2\mathrm{O} \quad (2)$$

–O– derives from chemically bonded/adsorbed oxides.

(3) Reaction contributing to capacity degradation with cycling process

$$\mathrm{Li}^+ + (\mathrm{EC} + \mathrm{EMC}\ldots) + \mathrm{e}^- \rightarrow \mathrm{SEI}\,(\mathrm{Li}_2\mathrm{CO}_3,\ \mathrm{ROCO}_2\mathrm{Li},\ \ldots) \quad (3)$$

$$\mathrm{LiPF}_6 + 2x\mathrm{Li}^+ + 2x\mathrm{e}^- \rightarrow \mathrm{Li}_x\mathrm{PF}_{5-x} + (x+1)\mathrm{LiF} \quad (4)$$

In addition to the reactions (3) and (4), the other contributing factors responsible for capacity degradation with cycle life arise out of particle fracture and loss of electrical contact between the electro-active species and current collector [33].

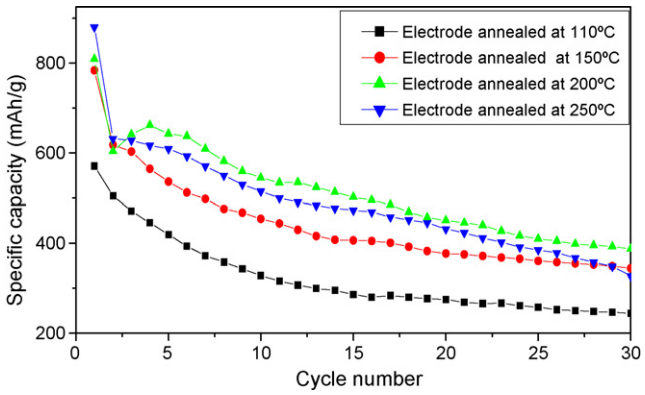

Fig. 4. Discharge capacity as a function of cycling with electrode annealing temperature.

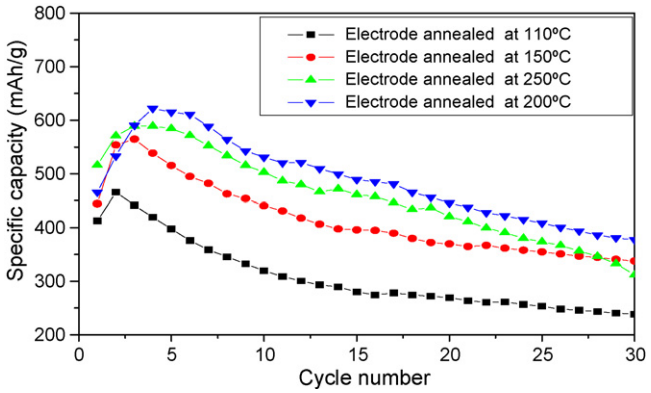

Fig. 5. Charge capacity as a function of cycling with electrode annealing temperature.

In the second cycle, the discharge and charge capacities respectively are 607 and 531 mAh g^{-1} which shows a considerable reduction in irreversible capacity to about 12%. The irreversible capacity in graphite electrode has been attributed to the formation of a passive film on graphite particles which comprises mainly LiF, Li_2CO_3 and Li_2O [20,22,34].

3.2.2. Capacity with cycle number at different electrode annealing temperatures

The discharge capacity of the annealed electrodes at different temperature on cycling is depicted as Fig. 4. The curve shows an improvement of discharge capacity (lithiation) as the annealing temperature increases which is evident from the high discharge capacity of 387 mAh g^{-1} delivered at 200 °C compared to 327 mAh g^{-1} at 110 °C at 30th cycle. The increase of capacity with annealing temperature implies the improvement of affinity among electro-active particles and also with current collector due to reinforcing property of the binder up to 200 °C and the decline of capacity at 250 °C reveals that further reinforcement of the particulate at higher temperature leads to deleterious effect that possibly arises out of loss of electrode porosity and increase of electrode resistance. Again between 11 and 30 cycles the fall of capacity shows an up trend as 3.5, 5.0, 7.5, and 8.8% with electrode annealing temperatures of 110, 150, 200 and 250 °C, respectively, suggesting that the annealing temperature not only increases the discharge capacity but also causes degradation of capacity with cycle number (reactions (3) and (4)). Fig. 5 illustrates charge capacity of electrodes annealed at different temperature on cycling. In all four curves the first charge capacity values for delithiation (charging) process remains at a low value, reaches a maximum and stabilizes in the subsequent cycles. The gain in charge and discharge capacity after the first cycles in all four temperatures except for 110 °C (Fig. 4) may be attributed to realignment of formed Li_2O along with other constituents of passive film followed by enhancement of electrical conductivity between particulates of the anode with cycling. The increase of reversible capacity with cycle number with electrode annealing temperature may be assumed as due to enhanced affinity of active materials with the current collectors. Further support for the improved capacity for high temperature annealed electrodes may be understood from the SEM picture which shows well separated electrode particulates with interspaces contributing enhanced lithium ion migration and better buffer action to accommodate the large volume change during cycling processes. Similar reports [13,14] on the capacity enhancement by annealing of electrode by Zuo et al. [15] for the SiMn/C anode, the improved reversible capacity (426 mAh g^{-1}) for the electrode annealed at 200 °C after 30 cycles has been observed. Fig. 6 shows the charge/discharge capacity and columbic efficiency with cycle number for the electrode annealed at 200 °C. The curve shows upon progressive cycling the columbic efficiency shows an improvement and remains between 95 and ~100%.

3.2.3. Irreversible capacity loss

Fig. 7 illustrates irreversible capacity loss exhibited by Fe–Cu–Si/C electrodes during first cycle (lithiation process) for the electrodes annealed at different temperatures. The curve shows a higher irreversible capacity for the electrodes annealed at >150 °C. The high temperature annealing causes better particle segregation aided by PVDF binder which makes easy diffusion of lithium ions and effective conversion of all oxides present in the electrode during initial discharge (reaction (2)). The high charge consumption [20] for SEI film formation in

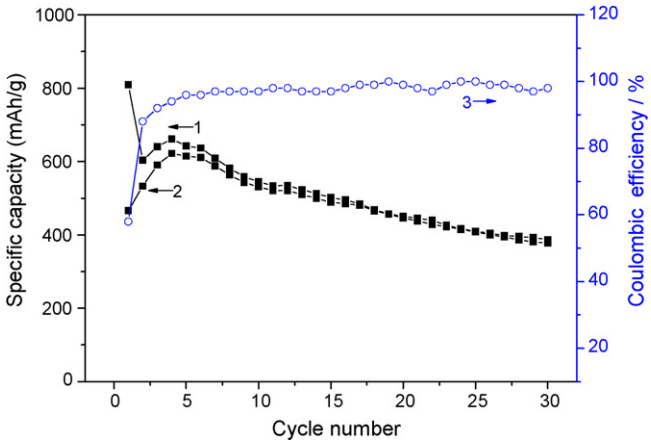

Fig. 6. Charge/discharge capacity and coulombic efficiency with cycle number for the electrode annealed at 200 °C: (1) discharge capacity (Q_1), (2) charge capacity (Q_2), (3) % of coulombic efficiency, ($Q_2 \times 100/Q_1$).

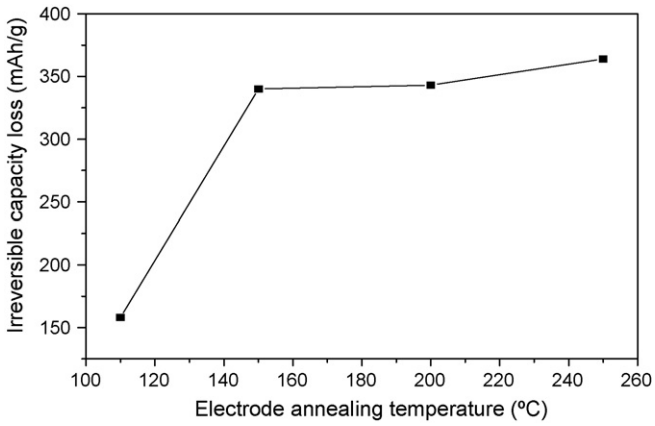

Fig. 7. Irreversible capacity loss as a function of electrode annealing temperature.

Cu–Si alloy [20] anode has been explained as due to increase of surface area through longer ball milling duration.

4. Conclusion

Phase characterizations of Fe–Cu–Si/C reveal that ball milling does not produce any alloy formation and the electrode constituents remain only in elemental states. The electrode annealing effected the reinforcement of electro-active particles resulting in particle segregation and enhanced affinity among the particles as well as with the current collector. The best performing electrode annealed at 200 °C exhibits high initial discharge and charge capacity of 809 and 464 mAh g^{-1}, respectively with a sustainable reversible capacity of ∼385 mAh g^{-1} at 30th cycle and maintains high coulombic efficiency of >95% after 4th cycle. For the electrode annealed at >200 °C, the electrode hardening begins leading to loss of porosity electrode resulting in decline of capacity. Higher electrode annealing temperature gave higher reversible as well as irreversible capacity. Finally it can be concluded that the new anode composition Fe–Cu–Si/C with higher reversible capacity can be an alternative anode material in place of graphite for lithium ion battery.

Acknowledgement

This work has been carried out at the Division of Advanced Batteries supported by NGE program (Project No. 1001653) of KERI, Korea. One of the authors A. Veluchamy wishes to thank the Korean Federation of Science and Technology Societies, Korea, for awarding Brain Pool Fellowship and also thanks to CECRI/CSIR, India for granting extraordinary leave.

References

[1] N. Dimov, S. Kugino, M. Yoshio, Electrochim. Acta 48 (2003) 1579.
[2] R. Yazami, K. Zaghib, M. Deschamps, J. Power Sources 52 (1994) 55.
[3] J. Wolfenstine, J. Power Sources 124 (2003) 241.
[4] G.X. Wang, L. Sun, D.H. Bradhurst, S. Zhong, S.X. Dou, H.K. Liu, J. Power Sources 88 (2000) 278.
[5] M.S. Park, S. Rajendran, Y.M. Kang, K.S. Han, Y.S. Han, J.Y. Lee, J. Power Sources 158 (2006) 650.
[6] M.S. Park, Y.J. Lee, Y.S. Han, J.Y. Lee, Mater. Lett. 60 (2006) 3079.
[7] Z. Wang, W.H. Tian, X.H. Liu, Y. Li, X.G. Li, Mater. Chem. Phys. 100 (2006) 92.
[8] M.S. Park, Y.J. Lee, S. Rajendran, M.S. Song, H.S. Kim, J.Y. Lee, Electrochim. Acta 50 (2005) 5561.
[9] H.Y. Lee, Y.L. Kim, M.K. Kong, S.M. Lee, J. Power Sources 141 (2005) 159.
[10] H.Y. Lee, S.M. Lee, J. Power Sources 112 (2002) 649.
[11] J.B. Kim, B.S. Jun, S.M. Lee, Electrochim. Acta 50 (2005) 3390.
[12] H. Dong, R.X. Feng, X.P. Ai, Y.L. Cao, H.X. Yang, Electrochim. Acta 49 (2004) 5217.
[13] P. Zuo, G. Yin, Y. Tong, Solid State Ionics 177 (2006) 3297.
[14] P. Zuo, G. Yin, J. Alloys Compd. 414 (2006) 265.
[15] P. Zuo, G. Yin, J. Zhao, Y. Mao, X. Cheng, P. Shi, T. Takumura, Electrochim. Acta 52 (2006) 1527.
[16] Y.L. Kim, H.Y. Lee, S.W. Jang, S.H. Lim, S.J. Lee, H.K. Baik, Y.S. Yoon, S.M. Lee, Electrochim. Acta 48 (2003) 2593.
[17] H. Kim, J. Choi, H.J. Sohn, T. Kang, J. Electrochem. Soc. 146 (1999) 440.
[18] G.A. Roberts, E.J. Cairns, J.A. Reimers, J. Power Sources 110 (2002) 424.
[19] J.W. Kim, J.H. Ryu, K.T. Lee, S.M. Oh, J. Power Sources 147 (2005) 227.
[20] Y. NuLi, B. Wang, J. Yang, X. Yuan, Z. Ma, J. Power Sources 153 (2005) 371.
[21] S. Yoon, S. Lee, H. Kim, H.J. Sohn, J. Power Sources 161 (2006) 1319.
[22] K. Wang, X. He, L. Mang, J. Ren, C. Jiang, C. Wan, Solid State Ionics 178 (2007) 115.
[23] X.D. Wu, Z.X. Wang, L.Q. Chen, X.J. Huang, Electrochem. Commun. 5 (2003) 935.
[24] Y.S. Lee, J.H. Lee, Y.W. Kim, Y.K. Sun, S.M. Lee, Electrochim. Acta 52 (2006) 1523.
[25] P. Patel, I.S. Kim, P.N. Kumta, Mater. Sci. Eng. B 116 (2005) 347.
[26] W.J. Weydanz, M. Who-Mehrens, R.A. Huggins, J. Power Sources 81–82 (1999) 237.
[27] M.D. Fleischauer, J.M. Topple, J.R. Dahna, Electrochem. Solid-State Lett. 8 (2005) A137.
[28] H. Dong, X.P. Ai, H.X. Yang, Electrochem. Commun. 5 (2003) 952.
[29] J. Zhang, J.L. Shui, S.L. Zhang, X. Wei, Y.J. Xiang, S. Xie, C.F. Zhu, C.H. Chen, J. Alloys Compd. 391 (2005) 212.
[30] J.N. Jayaprakash, N. Kalaiselvi, C.H. Doh, Intermetallics 15 (2007) 442.
[31] Z.N. Zhang, P.X. Huang, G.R. Li, T.Y. Yan, G.L. Pan, X.P. Gao, Electrochem. Commun. 9 (2007) 713.
[32] N. Kalaiselvi, C.H. Doh, C.W. Park, S.I. Moon, M.S. Yun, Electrochem. Commun. 9 (2004) 1110.
[33] D. Aurbach, A. Schechter, in: G. Abbas Nazri, G. Pistoia (Eds.), Lithium Batteries Science and Technology: Advanced Liquid Electrolyte Solutions, Kluwer Academic Publishers, Boston, 2004, p. 530.
[34] N.L. Rock, P.N. Kumta, J. Power Sources 164 (2007) 829.